TEMPERATURE PROFILE CALCULATION FROM EMISSION SPECTROSCOPY MEASUREMENTS IN NITROMETHANE SUBMITTED TO PLATE IMPACTS

V. Bouyer[1,2], G. Baudin[1], C. Le Gallic[1]
[1]French Ministry of Defense, DGA/DCE/Centre d'Etudes de Gramat
46500 Gramat, France

I. Darbord[2], P. Hervé[2]
[2] LEEE, Paris X University,
1, Chemin Desvallières, 92410 Ville d'Avray, France

A time-resolved emission spectroscopy technique has been developed for spectral analysis of NM submitted to plate impact in the spectral range 0.3-0.85 µm. It enables to obtain the optical characteristics of the different phases of the shock to detonation transition of NM. The emission spectra obtained clearly show the semi-transparency of the media involved. An absorption model of a carbon particles and water vapor mixture is studied in order to explain the radiance measurements. The determination of temperature profiles is carried out with the resolution of the equation of radiative transfer by an inversion method.

INTRODUCTION

To improve knowledge of the initiation and detonation of solid or liquid high explosives, temperature profiles determination in these materials during these dynamic phases gives precious information. This state variable is indeed of great interest for the understanding of the involved chemical kinetics and for the accuracy of hydrodynamic code related to condensed explosives. Its measurement is also obviously basic to characterize the thermal effects of high explosives. For many years a non-intrusive technique, optical pyrometry[1,2,3,4], has been used to measure the temperature during the shock to detonation transition (SDT) of a liquid explosive, nitromethane (NM), and during the detonation of very non-ideal high explosives. This technique has a response time of only a few nanoseconds, compatible with the swiftness of the phenomena. However the temperature determination, based on thermal radiation emitted by the explosive, requires an assumption on the emissivity of the material. This data is not measurable in such conditions of pressure (several GPa) and of temperature (several thousands of K). It is then supposed that it is a surface emissivity and that it linearly varies with the wavelength. In the case of NM and high explosive detonation products, the reaction and the detonation products are probably semi-transparent and the previous assumption, based on black or gray body theory, may then be unsuitable. Therefore, in order to get still more information on the optical properties of the initiation and detonation products, a time-resolved emission spectroscopy has been developed and applied to plane shock impacts of the reference explosive, NM. Temperature profiles can then be more precisely obtained.

EXPERIMENTAL CONFIGURATION

One interesting property of NM for optical studies is its semi-transparency. NM is transparent for wavelengths between 0.4 and 1.1 µm.

The experiments consist in plane shock impacts on explosive targets at 8.6 GPa, under conditions of one-dimensional strain. A single stage powder gun propels the projectile on the target at a velocity of 1940 m/s to initiate the detonation. The NM is in a polyethylene chamber of 25 mm depth, closed by a copper transfer plate[4,5,6]. An optical probe collects the thermal radiation emitted during the shock to detonation transition (SDT) through a lithium fluoride window. This radiation is transmitted to the spectroscopy system by an optical fiber. The light flux measured is the radiance emitted by the NM during the propagation of shock and detonation waves. The spectroscopy device has been described in previous papers[5,6]. The spectral and time resolutions obtained are respectively 32 nm (16 channels) and 1 ns; the spectral range studied is 0.3-0.85 μm.

Complementary measurement techniques are used: a polarization electrode records the shock entrance, the superdetonation and the detonation, piezo-electric pins measure the shock and detonation velocities.

RESULTS

We have performed several experiments of plate impacts at ~8.6 GPa on a 25 mm thick NM target (Table 1). V is the projectile velocity, P is pressure, t_1 is the formation of the superdetonation and t_2 the formation of the strong detonation.

TABLE 1. CHARACTERISTICS OF PLATE IMPACT SHOTS

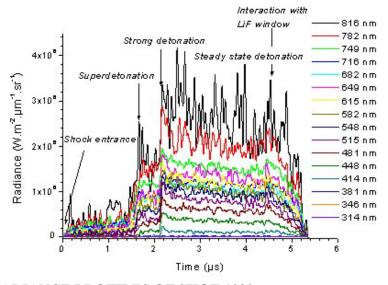| Shot Nb.	76	1020	1045	2019
V(m/s)	1926	1937	1936	1946
P(GPa)	8.37	8.64	8.64	8.7
t_1	1.7	1.65	1.38	1.6
t_2	2.36	2.15	1.84	2.15

FIGURE 1. RADIANCE PROFILES OF SHOT 1020

Figure 1 represents the radiance signals for 16 wavelengths versus time obtained during shot 1020. Time resolution is 20 ns after filtering through noise. These measurements, with the piezo-electric pins and electrode signals clearly show the different stages of the SDT as described by Chaiken[7].

Radiance temperature profiles have been calculated with the Planck law (Figure 2). The true temperature is at least equal to the maximum radiance temperature.
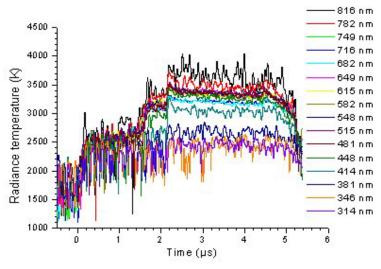
FIGURE 2. RADIANCE TEMPERATURE OF SHOT 1020

Changes in radiance depending on wavelength have been studied for various typical stages of the SDT (Figure 3).

From the formation of the superdetonation, a hollow appears between 0.65 and 0.75 μm. It remains until the end of the propagation of the detonation wave. This hollow characterizes semi-transparent optical properties.
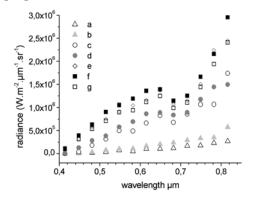

FIGURE 3. RADIANCE SPECTRA AT DIFFERENT TIMES: a) after shock entrance (0.3 μs), b) before the superdetonation formation (1.2 μs), c) superdetonation formation (1.65 μs), d) 1.9 μs, e) catch up of the shock wave (2.15 μs), f) strong detonation (2.45 μs), g) overdriven steady state detonation (3.8 to 4.4 μs). Radiance values were averaged around the given time value.

DISCUSSION

We studied the optical properties of the different states of the SDT.

Shock entrance

The evolution of the signal emitted after shock entrance leads to conclude that the shock is transparent. The radiance temperature after shock entrance is about 2500 K. It has been also recorded by pyrometry [4]. It is not in good agreement with Chaiken's model that predicts a shock temperature of about 1000 K. Multiple shocks experiments performed at CEG lead to the same results[8]. We explain this high temperature by local chemical reactions[4] (hot spots) due to heterogeneities at the impactor/explosive interface (Figure 4).
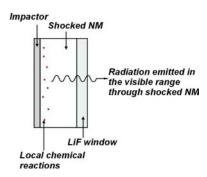

FIGURE 4. RADIATION EMITTED DURING THE PROPAGATION OF THE SHOCK

Sustained steady state detonation

The emitted radiation before the interaction with the LiF window is constant. It could be explained by a surface area emissivity of the detonation front. But the radiance temperature values during the detonation

propagation show a deviation of 500 K depending on the wavelengths (Figure 2). This implies that detonation products are semi-transparent. The constant signal is more likely due to the fact that the radiation comes from a small thickness behind the detonation wave, remaining constant during the propagation (Figure 5). Detonation products are called optically thick.
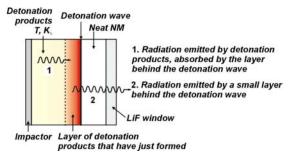

FIGURE 5. RADIATION EMITTED DURING THE PROPAGATION OF THE OVERDRIVEN DETONATION

We calculated the radiation emitted in this configuration and compared it to the radiation emitted by the entire cell, by using the equation of radiative transfer (ERT). According to CJ theory, the temperature profile behind the detonation front is constant. Thus, for a sustained steady state detonation, the ERT is [5]:

$$L_\lambda(\ell) = L_\lambda^0(T)(1 - e^{-K_\lambda(x_D - x_0)}) \qquad (1)$$

L_λ is the radiance at wavelength λ, L^0_λ is the black body radiance, T is the detonation products temperature, K_λ is the absorption coefficient, x_D and x_0 are the detonation and impactor/explosive interface positions, ℓ is the cell depth.

Figure 6 shows that when K_λ increases, the radiation emitted becomes constant and for the largest value of K_λ, the radiation is the same as the radiation emitted by a small layer of 5 mm thick behind the detonation front.

The detonation products are optically thick but their emissivity $\varepsilon = 1 - e^{-K_\lambda(x_D - x_0)}$ is lower than 1 so they do not behave like a black body.
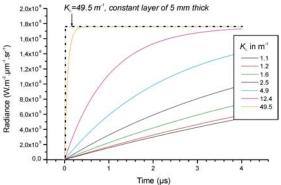

FIGURE 6. EFFECT OF K_λ ON THE RADIANCE

Superdetonation

The shock is transparent so we can measure the radiation emitted by the superdetonation wave. BMI measurements performed at the CEG show that the laser beam crosses the reaction products thickness: they are semi-transparent. By focusing on the propagation of the superdetonation on Figure 1, we can see that for wavelengths higher than 0.6 µm, the signal is constant whereas under 0.6 µm, it increases. In the first case, reaction products behind the superdetonation behave as steady state detonation products and in the second case, they are transparent. We can say that reaction products are optically thick in the spectral range 0.6-0.85 µm and optically thin in the range 0.4-0.6 µm.

MODEL FOR THE ABSORPTION COEFFICIENT

The results obtained on the optical properties of the reaction and detonation products lead us to try to find out which species cause the hollow in the radiance spectra. In the visible range, only the carbon clusters and water vapor emit thermal radiation. Data on optical properties at high pressures P and temperatures T does not exists. Our model is based on data at lower P and T.

Carbon clusters

Clusters size has been estimated to 50 Å[9]. Volume fraction of carbon in detonation products calculated with CHEETAH code is 6%. Therefore, the particles are in a dependent scattering regime that is difficult

to calculate. We chose in a first approximation the independent scattering regime that is Rayleigh scattering for small particles size. In this case, scattering is negligible and there is only absorption. The absorption coefficient of particles with refractive index n-iχ, and volume fraction f_v is [10]:

$$K_\lambda = \frac{36\pi n\chi}{(n^2-\chi^2+2)^2+4n^2\chi^2}\frac{f_v}{\lambda} \qquad (2)$$

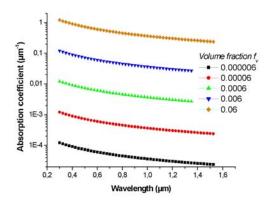Figure 7 shows K_λ calculation for several f_v values.

FIGURE 7. CALCULATION OF K_λ WITH EQUATION (2)

ERT of a scattering, emitting and absorbing medium becomes ERT of an emitting and absorbing medium so equation (1) can be used to calculate radiance emitted by detonation products.
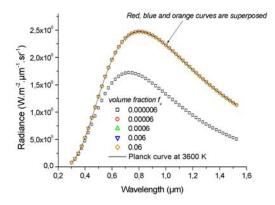

FIGURE 8. RADIANCE SPECTRA OF CARBON CLUSTERS IN RAYLEIGH SCATTERING REGIME

Figure 8 shows radiance values at the interaction of the detonation wave with the window at 3600 K. More accurate calculations show that we obtain the Planck curve at 3600 K for f_v values higher than 2.10^{-5}.

Water vapor

Table 2 presents absorption lines of H_2O in the visible range. The exponential wide band model of Edwards is used to represent the absorption coefficient[10]. For each line centered on λ_i:

$$K_{\lambda_i} = \frac{\alpha}{\omega}e^{-2\left|\lambda-\lambda_i\right|/\omega} \qquad (3)$$

ω is the line width and α is the intensity.

TABLE 2. POSITION AND INTENSITY OF ABSORPTION LINES OF H2O[11]

Wavelength (µm)	Intensity (a.u.)
0.698	0.2
0.724	1.08
0.823	0.93
0.906	2.4
0.942	10
0.977	2.1

Figure 9 shows the absorption coefficient of water vapor for several values of ω.
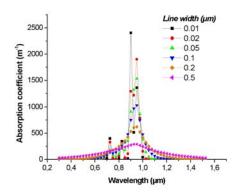

FIGURE 9. CALCULATION OF K_λ WITH EQUATION (3)

The calculation of the radiance emitted by a media only composed of water vapor behind the detonation front leads to Figure 10.
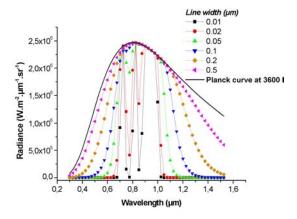
FIGURE 10. RADIANCE SPECTRA OF WATER VAPOR

Water vapor and carbon clusters in detonation products

We can now calculate the radiance of both water vapor and carbon. The absorption coefficient of the mixture is the sum of the absorption coefficient of water K_λ^{water} and the absorption coefficient of carbon K_λ^{carbon}. If the volume fraction is too high, the radiance curves will fit the Planck curve at 3600 K. If f_v is lower than 2.10^{-5}, it is the water absorption coefficient that will give the shape of radiance spectra. The carbon will create a continuous background (Figure 11).
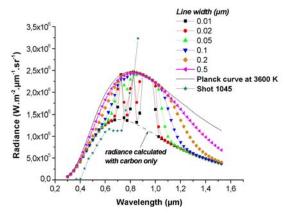

FIGURE 11. RADIANCE SPECTRA OF WATER VAPOR AND CARBON CLUSTERS

It has been difficult to fit the model with our emission spectroscopy measurements (see shot 1045 on Figure 11). For lower wavelengths, the shapes are closed but there is an intensity deviation and for wavelengths of about 0.8 μm, our measurements seem to fit to the water vapor line. Our model is maybe too simple. It is likely that the Rayleigh scattering independent model is not valid. Moreover, we chose the simplest model for water vapor emission and we do not know the changes of the spectrum with increasing pressures and temperatures. Moreover, the uncertainty on the volume fraction of carbon particles is high. With 6% of carbon, as calculated by CHEETAH code, the calculated radiance fit with Planck curve at the same temperature whereas we showed previously that the medium was semi-transparent. The hypothesis of an emitting and absorbing medium is perhaps not adapted. Hence, the emitted radiation is not only thermal radiation. In Gruzdkov and Gupta works[12], the emission spectrum between 0.4 and 0.75 μm of NM shocked at 16.7 GPa under a stepwise loading process has been measured, and a peak appeared at 0.65 μm. They explained it as luminescence from reaction products, maybe NO_2. NO_2 spectrum shows lines around 0.83 μm and between 0.5 and 0.6 μm[13]. Fluorescence phenomena from NO_2 or other species like N_2 could take place at these wavelengths.

TEMPERATURE PROFILE DETERMINATION

We are presenting here a method to determine temperature profiles during the SDT from the emission spectroscopy measurements. It is based on the resolution of the ERT by an inversion method.
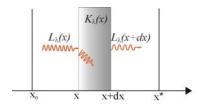

FIGURE 12. EMMITING AND ABSORBING MEDIUM

Given a semitransparent medium at a temperature T, with an absorption coefficient K_λ and a thickness (x^*-x_0), the ERT is:

$$L_\lambda(x^*)=L_\lambda(x_0)\exp\left(-\int_{x_0}^{x^*}K_\lambda(x)dx\right)$$

$$+\int_{x_0}^{x^*}K_\lambda(x')L_\lambda^0(T)\exp\left(\int_{x'}^{x^*}-K_\lambda(x)dx\right)dx' \quad (4)$$

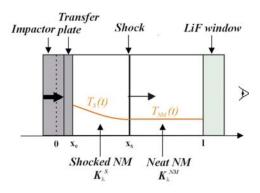We applied as an example the ERT to the first step of the SDT, the propagation of the shock in the cell:

FIGURE 13. SHOCK PROPAGATING IN NM

The ERT becomes:

$$L_\lambda(\ell)=L_\lambda^S(x_S)\exp\left[-\int_{x_S}^{\ell}K_\lambda^{NM}(x)dx\right]$$

$$+\int_{x_S}^{\ell}K_\lambda^{NM}(x')L_\lambda^0(T_{NM})\exp\left[-\int_{x'}^{\ell}K_\lambda^{NM}(x)dx\right]dx'$$

with $\qquad\qquad\qquad\qquad\qquad\qquad (5)$

$$L_\lambda^S(x_S)=L_\lambda(x_0)\exp\left[-\int_{x_0}^{x_S}K_\lambda^S(x)dx\right]$$

$$+\int_{x_0}^{x_S}K_\lambda^S(x')L_\lambda^0(T_S)\exp\left[-\int_{x''}^{x_S}K_\lambda^S(x)dx\right]dx'$$

The inversion of this equation should give the temperature profile $T_S(t,x)$ in the cell as well as $K_\lambda^S(t,x)$ (t is time and x is position).

The difficulties of the inversion of ERT are:

- how many information do the radiance measurements contain, related to the temperature and the absorption coefficients that are still unknown?
- which parameterization should we choose to represent T and K_λ ?

The proposed method is in two steps: first, a sensitivity analysis to the physical parameters T and K_λ is made. Then, a least squares algorithm carries out the identification.

Sensitivity analysis

The function to be retrieved is F: $\Theta\rightarrow L_\lambda$, with Θ the T and K_λ parameters vector. The sensitivity analysis consists in studying the derivative of the function F, F'=$dL_\lambda/d\Theta$, and finding the singular values of F'. The singular values are a diagonal matrix and the study of the decrease of the values enables to predict the number of independent parameters.

If we represent T and K_λ as vectors $T_{k,i}$ and $K_{k,i,j}$, (where k is time increment, i space increment and j wavelength increment), the problem will have too many parameters to be precisely determined. This kind of parameterization is called *thin*. Therefore, we need to reduce the number of parameters by adding information on T and K_λ. That's why we decided to test the method on known temperature profiles T(t,x) and by calculating the shape of $K_\lambda(t,x)$ at different temperature using our radiance measurements and the simple equation (1).

The shape of the absorption coefficient deduced from the previous analysis is given by Figure 14.
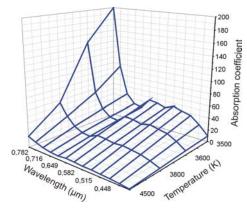

FIGURE 14. SHAPE OF THE ABSORPTION COEFFICIENT OF REACTION PRODUCTS

3 levels of parameterization using this shape have been chosen:

1. the values at the nodes of the grid are independent,
2. the values in the grid are function of the values on the axis,
3. the shape is preserved, only the position on the grid in Z axis changes.

The parameterization is a linear interpolation of the values of the grid. At each level, the number of parameters is reduced but each parameter contains more information. This interpolation links the neat NM state to the shocked NM state and the shocked state to the reacted explosive state as shown on Figure 15.
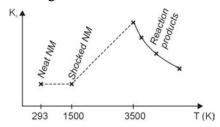

FIGURE 15. K_λ LINEAR INTERPOLATION

It is likely that this interpolation is not representing the reality and we will have to take this into account when analyzing the results.

The first studied temperature profiles are presented Figure 16. The parameterization of the temperature is based on the shape of case 1 and case 2 and is called *red (*for reduced).
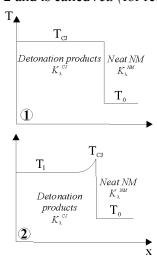

FIGURE 16. TEMPERATURE PROFILES

The results of the sensitivity analysis are shown on Figure 17 (T, temperature, k, absorption coefficient). Only the 20 first singular values are represented.

For a given noise level, the number of values higher than this level gives the number of parameters that can be determined. In most of the cases, 20 singular values can be determined.

Thin parameterization cannot be used because it is too complex to resolve. We can see that reducing the total number of parameters with thin parameterization of T does not lose information. Moreover, comparing parameterization 1 and 2, the 16 first values are the same. Therefore, the reduction of the number of parameters for K_λ does not also lose information.
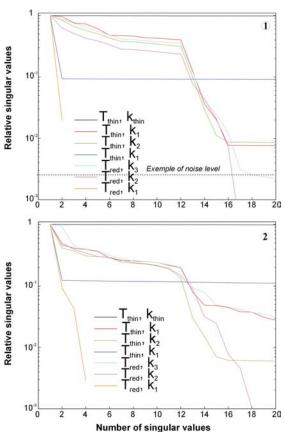

FIGURE 17. SINGULAR VALUES FOR CASES 1 AND 2

Inversion

The inversion is carried out with a least square approach. The quadratic criterion J to be minimized is:

$$J(L^{cal}) = \frac{1}{2} \sum_{k,j} \left(\frac{L_j^{mes,k} - L_j^{cal,k}}{\sigma_j^k} \right)^2 \qquad (6)$$

L^{cal} is radiance calculated with ERT, L^{mes} is measured radiance and σ stands for the noise and relative errors of measurements. In the 2 cases presented here, L^{mes} will be calculated from temperature profiles of Figure 16.

The sensitivity analysis is a local analysis, performed around the searched value. A good sensitivity does not guarantee that the problem will be solved without finding local minima that are not the solution of the problem. For example, Figure 18 shows the drawing of the least square criterion J for case 1. Depending on the chosen parameterization and on the initial point of the inversion algorithm, we can find local minimum (red curve).
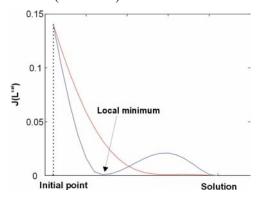

FIGURE 18. EXAMPLE OF LOCAL MINIMUM

The diagram on Figure 19 explains the method used to find out inversion results for cases 1 and 2.
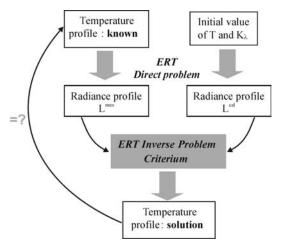

FIGURE 19. INVERSION METHOD OF KNOWN TEMPERATURE PROFILES

The inversion method is validated if the deviation between known temperature that is used to calculate radiance and the solution is low, i.e. low deviation between L^{cal} and L^{mes}.

Results of inversion for case 1 and case 2 are given in Table 3.

TABLE 3. RESULTS OF INVERSION

Case 1		
Parameterization	Initial T (K)	T_{CJ} (K)
d1	3000	**3592**
h3	3000	3601
h2	3601	3601
h1	3601	**3600**
d_1	4500	**3600**
h_3	4500	3782
h_2	3782	3600
h_1	3600	**3599**

Case 2		
Parameterization	Initial T (K)	T_{CJ}/T_I (K)
d_1	3250/2500	**3251/2940**
h_3	3250/2500	3250/2810
h_2	3250/2810	3486/3146
h_1	3486/3146	**3486/3183**
d_1	4500/3250	**4369/2877**
h_3	4500/3250	4500/3080
h_2	4500/3080	4500/3168
h_1	4500/3168	**4500/3148**

In case 1, $T_{CJ}=3600$ K is the temperature to be determined.

In case 2, $T_{CJ}=3500$ K, $T_I=3000$ K.

We chose the reduced parameterization for T. d_1 corresponds to parameterization 1 of K_λ. The parameterization h_1, h_2, and h_3 are coupled: we begin by using h_3 (parameterization 3 of K_λ). The results of h_3 are used as initial point for h_2 (parameterization 2 of K_λ) and then, the results of h_2 are used as initial point for h_1.

In case 1, the solution is the same as the searched value 3600 K. Optimisation with $h_{3,2,1}$ seems to give better results than with d_1. But in case 2, if the initial point is to far from the searched values (3500/3000), the inversion solution does not give good results. Therefore, the method is not yet efficient on profile 2 and on more complex profiles. The difficulty is linked to the parameterization of T.

CONCLUSION

Time-resolved emission spectroscopy performed during the detonation of NM gives radiance measurements versus time between 0.3 and 0.85 µm, with a 28 nm spectral resolution. Our results showed a discontinuity between 0.65 and 0.75 µm in the radiance profile, appearing from the formation of the superdetonation. This is characteristic of semi-transparency. Shocked NM remains transparent. Reaction products are optically thin in the range 0.4-0.6 µm and optically thick in the range 0.6-0.85 µm. Detonation products are also optically thick in the visible range. The monochromatic absorption coefficient of detonation products depends on wavelength and does not correspond to the emissivity of a black body. An absorption model based on the emission of carbon particles and water vapour is proposed. It is difficult to fit the model to emission measurements because of lack of data at high pressures and temperatures. The determination of temperature profiles by an inversion method has been performed and is currently validated on the case of a steady state detonation. The validation on the experimental case is in progress.

REFERENCES

1. Kato Y., Mori N., Sakai H., Detonation temperature of nitromethane and some solid high explosives, in 8th Symposium on detonation, Albuquerque, NM, 1985, pp. 558-566.
2. Léal Crouzet B., Ph. D. Dissertation, University of Poitiers, France, 1998.
3. Léal Crouzet B., Baudin G., Presles H.N., Combustion and Flame 122, 463-473 (2000).
4. Léal B, Baudin G., Goutelle J.C., Presles H.N., An optical pyrometer for time resolved temperature measurements in detonation wave, 11th symposium on detonation, 1998, pp. 353-361.
5. Bouyer V., Baudin G., Le Gallic C., Hervé P., Emission Spectroscopy Applied to Shock to Detonation Transition in Nitromethane, 12th APS Topical Group Meeting on Shock Compression of Condensed Matter, Atlanta, 2001, pp. 1223-1226.
6. Bouyer V., Time-resolved emission spectroscopy measurements in nitromethane submitted to plate impacts, 52nd Aeroballistic Range Association, Québec, 2001.
7. Chaiken R. F., The kinetic theory of detonation of high explosives, M.S Thesis, Polytechnic Inst. of Brooklyn, 1957.
8. Baudin G., Serradeil R., Le Gallic C., Bouinot P., Comportement sous choc du nitromethane, technical report, CEG, 2002.
9. Winter N. W., Ree F. H., Stability of the graphite and diamond phases of finite carbon clusters, 11th symposium on detonation, 1998, pp. 480-489.
10. M. F. Modest, Radiative Heat Transfer, Mc Graw-Hill International Editions, 1993.
11. Smith F. G. eds., Atmospheric propagation of radiation, SPIE Optical Engineering Press, 1993.
12. Gruzdkov Y. A., Gupta Y. M., J. Phys. Chem. A 102, 2322-2331 (1998).
13. Herzberg G., Molecular spectra and molecular structure, vol. III Electronic spectra and electronic structure of polyatomic molecules, Masson, 1992.